Journal of the Korean Physical Society, Vol. 72, No. 5, March 2018, pp. 555∼560

BER Analysis of Coherent Free-Space Optical Communication Systems with a Focal-Plane-Based Wavefront Sensor

Jingtai Cao
Changchun Institute of Optics, Fine Mechanics and Physics, Chinese Academy of Sciences, Changchun 130033, China and College of Communication Engineering, Jilin University, Changchun 130012, China

Xiaohui Zhao, Wei Liu and Haijun Gu*
College of Communication Engineering, Jilin University, Changchun 130012, China

(Received 4 September 2017, in final form 14 November 2017)

A wavefront sensor is one of most important units for an adaptive optics system. Based on our previous works, in this paper, we discuss the bit-error-rate (BER) performance of coherent free space optical communication systems with a focal-plane-based wavefront sensor. Firstly, the theory of a focal-plane-based wavefront sensor is given. Then the relationship between the BER and the mixing efficiency with a homodyne receiver is discussed on the basis of binary-phase-shift-keying (BPSK) modulation. Finally, the numerical simulation results are shown that the BER will be decreased obviously after aberrations correction with the focal-plane-based wavefront sensor. In addition, the BER will decrease along with increasing number of photons received within a single bit. These analysis results will provide a reference for the design of the coherent Free space optical communication (FSOC) system.

PACS numbers: 42.55.Tv, 42.68.Bz, 42.25.Bs, 42.15.Dp
Keywords: FSOC system, Atmospheric turbulence, Focal-plane-based wavefront sensor, BER
DOI: 10.3938/jkps.72.555

I. INTRODUCTION

Free space optical communication (FSOC) systems play a significant role in modern communication because they have some advantages over traditional microwave communications and conventional radio frequency, such as high communication speed, free license spectrum, and excellent security. They can be considered as an important supplement for traditional wireless communication systems and fiber optics communication systems. Recently, coherent FSOC systems have attracted more attentions due to their higher sensitivity, longer relay distance, larger communication capacity, and better receiver selectivity [1–4]. Though coherent FSOC systems have many advantages, they are still sensitive to atmospheric turbulence, because the wavefront phase and amplitude of the laser carrier signal are distorted by this turbulence with time through an atmospheric channel, which will obviously increase the system's bit-error-rate (BER). Fortunately, the developments of adaptive optics (AO) can compensate for this weakness of coherent FSOC systems by successfully correcting the turbulence-induced wavefront aberrations of the received laser carrier signal [5–9].

A closed-loop AO system applies an effective method to reduce the effects of atmospheric turbulence by correcting the wavefront aberrations in real time [7,8]. The AO system consists of a wavefront sensor, wavefront controller, and wavefront corrector. The wavefront sensor is one of most important units for the AO system. Its measurement precision directly decides the performance level of the AO system. The Shack-Hartmann wavefront sensor (SH-WFS) is the most widely used sensor [10–12]. However, because the scintillation of a laser is stronger than white light and the power of the laser carrier signal is reduced by multiple spectroscopes, the SH-WFS is not a system that should be used under strong scintillation conditions, especially in near-ground remote transmission [13–18].

For improving the efficiency of the wavefront sensor, research a wavefront sensing, has become a hot topic, such as sensor-less AO technology, holographic sensor and so on. Many researchers use a sensor-less AO unit to compensate for the wavefront aberrations for coherent FSOC systems. However, its control bandwidth and sensing accuracy are not sufficient [19–23]. The holographic senor which had advantages in sensing efficiency

*E-mail: ghyciom@163.com; Fax: +86-431-8515-2181

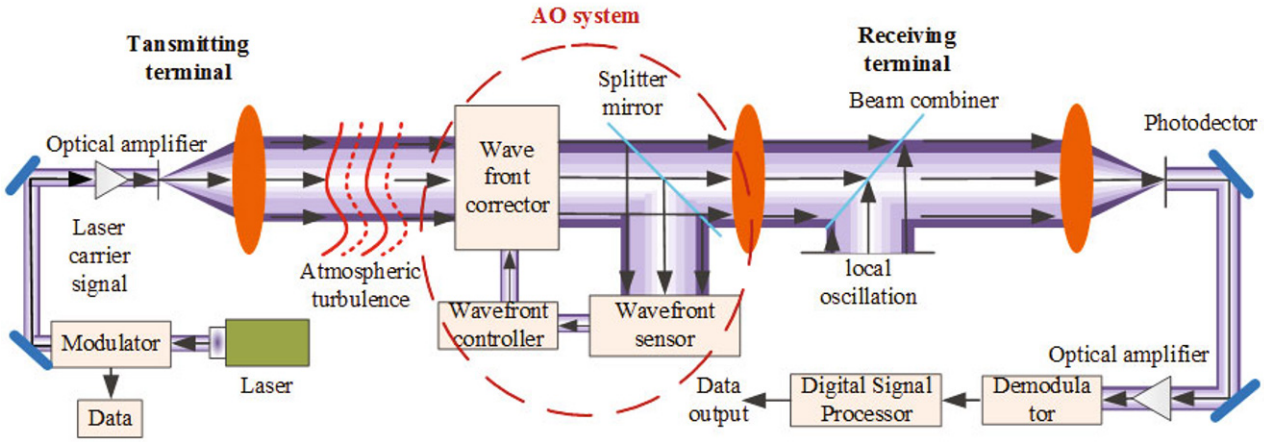

Fig. 1. (Color online) Schematic of the coherent FSOC system.

was proposed recently. However, it was more suitable for weak turbulence [24]. Focal-plane-based wavefront sensor was proposed in our previous works. The improvement in the FSOC performance with intensity modulation/direct detection (IM/DD) is discussed in detail. The results show that the coupling efficiency and the BER improvements are significant [25]. In this paper, we will analyze the BER performance for a coherent FSOC system on the basis of theory and a model analysis.

This paper is organized as follows: Sec. II provides the model of the FSOC communication system; then, the theory of a focal-plane-based wavefront sensor is given in brief based on our previous works. Finally, the BER expression for coherent FSOC systems is given. Sec. III gives the analytical results for the BER performance of coherent FSOC communication systems with a focal-plane-based wavefront sensor. Finally, the conclusions are given in Sec. IV.

II. MODEL ANALYSIS

1. Coherent FSOC communication system model

A coherent FSOC system with an AO unit is illustrated in Fig. 1. In this system, the laser source emits a laser beam modulated to be a laser carrier signal. Then, it is transmitted through an atmospheric link and arrives at a receiving terminal. Its frequency is mixed with the local oscillation signal to generate an intermediate frequency signal. A demodulator and a digital signal processer complete the subsequent processing. Here, an AO unit is introduced to compensate for the influence of atmospheric turbulence, which disturbs both the wavefront and the amplitude of the laser carrier signal during signal transmission. The AO unit consists of three parts: wavefront sensor, wavefront corrector, and wavefront controller. The wavefront sensor can measure the wavefront aberrations caused by the atmospheric turbulence. The wavefront controller controls the wavefront corrector according to the wavefront aberrations measured by using the wavefront sensor. The wavefront corrector performs the wavefront correction [6].

2. Focal-plane-based wavefront measurement model

In our previous work, we analyzed the coupling efficiency and the BER performance by using a focal-plane-based wavefront measurement for FSOC system based on IM/DD modulation [25]. In this paper, we discuss the BER performance improvement of a coherent FSOC system by using focal-plane-based wavefront measurement. Similarly, assume the receiving antenna of the FSOC system and the atmosphere can be assumed to compose a linear time-invariant system [25]. The system of Gaussian imaging formula is [25]

$$d(x) = f(x) * h(x) + n(x), \tag{1}$$

where $d(x)$, $h(x)$ and $f(x)$ denote the target image, the point spread function, and the ideal target image respectively, and $n(x)$ denotes the Gaussian noise. We adopt an additive white Gaussian noise model in this system.

According to previous work, the wavefront measurement method obtains wavefront aberrations by adopting two-channel laser carrier signal images, including the focal channel and the defocused channel, when the amount of defocusing is known, which is taken as a known phase difference. Meanwhile, the focal channel is the channel in which imaging plane is in the focal plane of the optical system, and the defocused channel is the channel in which the phase differences between the imaging plane and the focal plane of optical system are known [25]. The laser carrier signal imaged in the two channels can

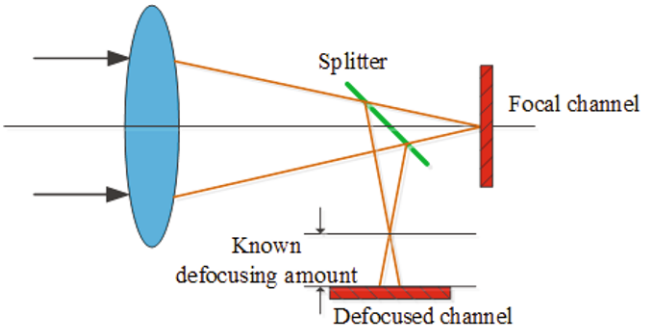

Fig. 2. (Color online) Sketch of the focal-plane-based wavefront sensor.

be expressed by using a Fourier transform as [25]

$$D_{\text{infocus}}(u) = F(u)H_{\text{infocus}}(u) + N_{\text{infocus}}(u) \quad (2)$$
$$D_{\text{defocus}}(u) = F(u)H_{\text{defocus}}(u) + N_{\text{defocus}}(u), \quad (3)$$

where $D_{\text{infocus}}(u)$, $H_{\text{infocus}}(u)$ and $N_{\text{infocus}}(u)$ are the frequency domain of the target image, the point spread function, and the noise in the focal plane channel respectively; additionally, $D_{\text{defocus}}(u)$, $H_{\text{defocus}}(u)$ and $N_{\text{defocus}}(u)$ are the frequency domain of the target image, the point spread function and the noise in the defocused channel. A sketch of a focal-plane-based wavefront sensor is shown in Fig. 2.

According to the Fourier optical theory, the relationship between the point spread function and the pupil function is shown as:

$$H(u) = P(u) \otimes P(u), \quad (4)$$

where $\otimes$ is the autocorrelation operator, $P(u)$ is the pupil function, which is given as

$$P(u) = A(u)e^{i(\phi(u))} \quad (5)$$

with $A(u)$ being the amplitude function of the pupil functionand the aberrations $\phi(u)$ can be expressed as the Zernike polynomials [26]

$$\phi(u) = \theta(u) + \sum_{m}^{M} \alpha_m Z_m(u) \quad (6)$$

with $Z_m(u)$ denoting the mth Zernike polynomial and α_m the corresponding weighting coefficient, and $\theta(u)$ a known aberration. Thereby, we can obtain the unknown aberration $\phi(u)$ by calculating α_m and then obtain the point spread function $h(x)$ by using Eq. (5) and Eq. (6).

In the Gaussian noise model, the mean-square deviation between the target image and the images of the two channels can expressed by using the likelihood function [25]

$$L(u,\alpha) = \sum_{u}(|D_{\text{infocus}}(u) - F(u)H_{\text{infocus}}(u,\alpha)|^2 + |D_{\text{defocus}}(u) - F(u)H_{\text{defocus}}(u,\alpha)|^2). \quad (7)$$

Based on the maximum likelihood estimate, we can obtain the target formulation, which has no correlation to the real target,

$$L_M(u,\alpha) = -\sum_{u} \frac{|D_{\text{infocus}}(u)H_{\text{defocus}}(u,\alpha) - D_{\text{defocus}}(u)H_{\text{infocus}}(u,\alpha)|^2}{|H_{\text{infocus}}(u,\alpha)|^2 + |H_{\text{defocus}}(u,\alpha)|^2}. \quad (8)$$

Furthermore, we can get the minimal corresponding weighting coefficient of the Zernike polynomials by using the Newton iteration method. Therefore, we can obtain the wavefront aberrations with the formulas provided by theory analysis. In real system, the wavefront corrector is used to correct the wavefront aberrations. For instance, a continuous surface deformable mirror is usually used in the FSOC system to correct for the wavefront aberrations in order to improve the communication performance [9]. In this paper, we use numerical simulation to realize the image acquisition, the wavefront aberrations calculation and the phase compensation of the laser carrier signal based on both of the focal plane channel and the defocus channel.

3. BER analysis model

On basis of our previous works, for the coherent FSOC system, BER is given by [9]

$$\text{BER} = \frac{1}{2} erfc\left(\frac{Q}{\sqrt{2}}\right), \quad (9)$$

where $erfc(\cdot)$ is the complementary error functionand $Q = \sqrt{\text{SNR}}$, where SNR is the signal-to-noise ratio of homodyne detection. For a synchronous binary-phase-shift-keying (BPSK) modulation system, the optical power at the receiver is [9]

$$P_S = N_P h\nu B. \quad (10)$$

Table 1. Zernike aberrations of the introduced wavefront.

Zernike item	Value	Zernike item	Value
4^{th} item	−0.0366	12^{th} item	0.0025
5^{th} item	0.0168	13^{th} item	−0.0281
6^{th} item	−0.1716	14^{th} item	0.1127
6^{th} item	0.0917	15^{th} item	−0.0229
8^{th} item	0.0127	16^{th} item	0.0849
9^{th} item	0.1486	17^{th} item	0.0138
10^{th} item	0.0672	18^{th} item	−0.0109
11^{th} item	−0.0822		

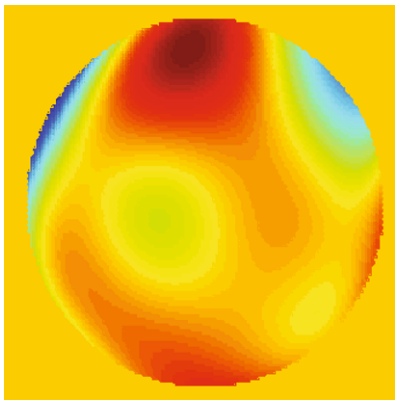

Fig. 3. (Color online) Distribution of the introduced wavefront.

The signal-to-noise ratio without atmospheric turbulence is [9]

$$\mathrm{SNR}_0 = \frac{2\delta P_S}{h\nu B} = 2\delta N_p, \tag{11}$$

where SNR_0 is the signal-to-noise ratio without atmospheric turbulence, N_p is the number of photons received within a single bit, and δ is the quantum efficiency of the detector. The BER of a homodyne receiver with BPSK modulation is [9]

$$\mathrm{BER} = \frac{1}{2} erfc(\sqrt{2\delta N_P \eta}), \tag{12}$$

where η is the mixing efficiency of the coherent FSOC system. Based on previous works, the mixing efficiency is approximately the Strehl ratio of far-field images and it is defined by the ratio of the far field encircled energy to the diffraction-limited encircled energy [9].

III. NUMERICAL SIMULATIONS

On basis of our previous works, in this research, we used the wavefront sensing method based on the focal plane through numerical simulations. Firstly, we obtain two simulated laser carrier signal images by adding known random aberrations, one being in the focal channel and the other in the defocused channel. Secondly, we obtain the wavefront aberrations by using focal-plane-based wavefront sensing. Finally, we discuss the BER performance of coherent FSOC systems in detail according to several experimental results.

Table 2. Zernike aberrations of the reconstruction wavefront.

Zernike item	Value	Zernike item	Value
4^{th} item	−0.0400	12^{th} item	0.0037
5^{th} item	0.0134	13^{th} item	−0.0316
6^{th} item	−0.1733	14^{th} item	0.1125
6^{th} item	0.0946	15^{th} item	−0.0231
8^{th} item	0.0164	16^{th} item	0.0855
9^{th} item	0.1522	17^{th} item	0.0127
10^{th} item	0.0679	18^{th} item	−0.0118
11^{th} item	−0.0843		

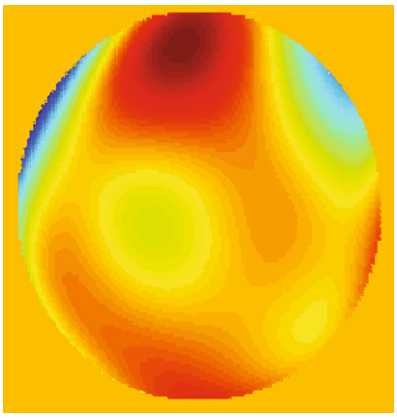

Fig. 4. (Color online) Distribution of the reconstruction wavefront.

In this paper, we select the wavelength as 1060 nm. The pixel size in our simulations is 9.9 μm, the aperture of transmitter and receiver is 0.2 m, the focal length of the transmitter and receiver is 3.7 m, and the diameter of the single mode fiber is nearly 10 μm. The propagation distance is 2 km, wind speed is 5 m/s, detector sampling time is 40 ms, and detector noise is 5 e. Here, refractive index structure constant is assumed to be 10^{-18} $\mathrm{m}^{-2/3}$ and the exposure time to be 500 μs. The receiver adopts a homodyne detector, and the system is based on BPSK modulation. We introduce random Zernike aberrations (only considering the 4^{th} to 18^{th} Zernike aberrations). In this paper, we only discuss the wavefront aberrations caused by atmospheric turbulence, ignoring other influences. The Zernike aberrations randomly introduced are shown in Table 1.

The wavefront distribution of the introduced aberrations is shown as Fig. 3. According to Fig. 3, the root-mean-square (RMS) value and the peak-to-valley (PV) value of the introduced aberrations are 0.3066 wave-

Table 3. RMS and PV values of the reconstruction wavefront.

RMS value (wavelengths)	PV value (wavelengths)
0.3118	2.4196

Table 4. Results of several experiments.

Num.	Introduced Aberrations RMS (wavelenghs)	Calculated Aberrations RMS (wavelengths)	Residual RMS (wavelenghs)
1	0.3036	0.3018	0.0023
2	0.4059	0.4084	0.0040
3	0.2403	0.2432	0.0039
4	0.3620	0.3615	0.0043
5	0.3589	0.3636	0.00550
6	0.3829	0.3829	0.0032
7	0.3812	0.3639	0.0075
8	0.2867	0.2837	0.0026
9	0.3110	0.3109	0.0021
10	0.3066	0.3118	0.0022
Mean	0.3339	0.3332	0.0038

(a)Focal channel image (b)Defocused image (c)Reconstruction image

Fig. 5. Images of the double channel and the reconstruction.

lengths and 2.3640 wavelengths, respectively. In this paper, we assume the defocusing between the focal channel and the defocused channel to be 0.5 mm. According to the two images, one of the focal channel and the other of the defocus channel, we can obtain the reconstructed wavefront expressed by the Zernike mode, which is shown in Table 2.

The distribution of reconstructed wavefront is shown in Fig. 4. Comparing Fig. 3 and Fig. 4, we see the distribution trends are consistent. The RMS and the PV values of the reconstructed wavefront are shown in Table 3. Similarly, the statistical features of wavefront aberrations are consistent between the introduced and the reconstructed wavefront aberrations. Images of focal channel and the reconstruction are shown in Fig. 5. As shown in Fig. 5, the reconstruction image with a high energy concentration is consistent with the focal channel image.

The RMS value of the residual aberrations is an important indicator to evaluate a wavefront sensing method.

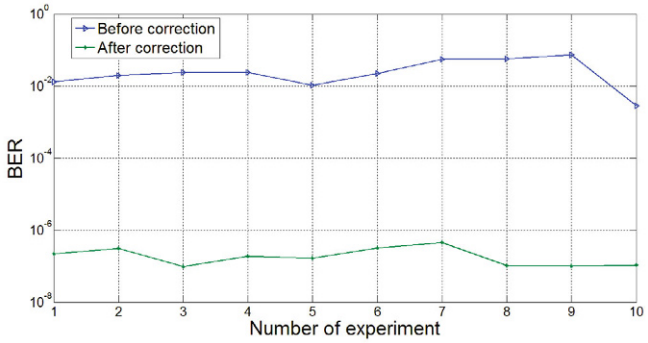

Fig. 6. (Color online) Results for BER when $N_p = 10$.

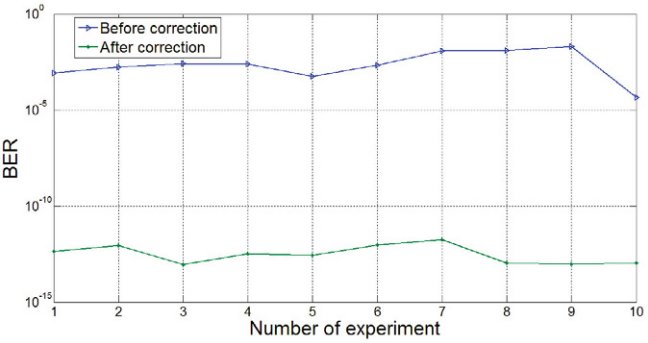

Fig. 7. (Color online) Results for BER when $N_p = 20$.

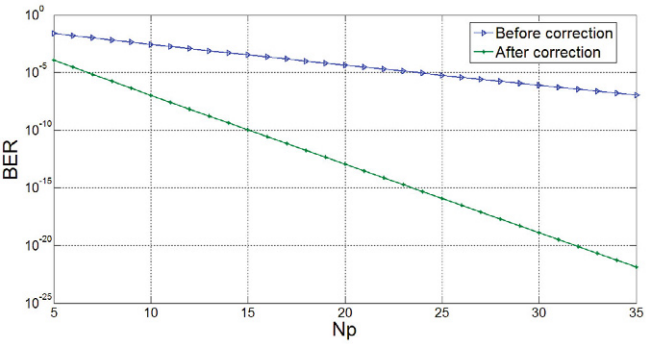

Fig. 8. (Color online) Relationship between the BER and N_p.

According to Table 1 and Table 2, the RMS value of residual aberrations is 0.0023. Thus, the focal-plane-based wavefront sensing is accurate enough to the reconstruct wavefront. The results are consistent with our previous work. In addition, we analyze the BER performance of coherent FSOC systems for several experimental results, which are shown in Table 4. As shown in Table 4, the mean of residual aberrations RMS value is about 0.002 wavelengths. Images of the focal channel and the reconstruction are shown in Fig. 5.

Considering that the mixing efficiency is approximately the Strehl ratio of far-field images, we can get the BER according to Eq. (12). Here, we assume the

quantum efficiency of the detector to be given by $\eta = 1$ and the number of photons received within a single bit to be given by $N_p = 10$. We only discuss a homodyne receiver in this paper. The results for the BER are shown in Fig. 6, according to several experimental results. As shown in Fig. 6, the BER is nearly 10^{-2} before correction and decrease to 10^{-5} after aberrations correction with the focal-plane-based wavefront sensor. Here, the aberrations correction compensates for the aberrations according to the results calculated by using the focal-plane-based wavefront sensor.

In a practical system, the number of photons received within a single bit can increase to 20 through an improved system design. The results with $N_p = 20$ are shown in Fig. 7. In addition, we give the results for the BER performances before and after correction with different N_p for one experimental result in Fig. 8. As shown in Fig. 8, the BER will obviously decrease with increasing N_p. When N_p is above 15, the BER will decrease below 10-9 after aberrations correction.

IV. CONCLUSION

In this paper, we analyze the BER performance of a coherent FSOC system with a focal-plane-based wavefront sensor on the basis of our previous works. Firstly, the theory of focal-plane-based wavefront sensing is introduced in brief. Then, the expression of BER for a homodyne detector with BPSK modulation is given. The expression shows that BER is related to the mixing efficiency. According to previous works, the mixing efficiency is approximately the Strehl ratio of far-field images. Thus, we analyze the BER performance by using images of the focal channel and the reconstruction. The results show that the BER is obviously decreased after corrections of the aberrations. Finally, the relationship between BER and N_p is given in Fig. 8. As shown in Fig. 8, after correction, the BER will decrease below 10^{-9} when N_p increases above 15.

However, our works only analyze the BER performance by using numerical simulation. In future work, we will design an experimental system to verify our analysis results in our simulation works. In addition, we will analyze the performance of coherent FSOC systems based on focal plane under different scintillation conditions.

ACKNOWLEDGMENTS

This work was supported by the China Postdoctoral Science Foundation (2016M590255) and by the National Natural Science Foundation of China (No. 61601195 and No. 61605199).

REFERENCES

[1] M. Jing, M. Lie, Y. Qingbo and R. Qiwen, Appl. Opt. **54**, 7575 (2015).
[2] S. Bonora and R. J. Zawadzki, Opt. Lett. **38**, 4801 (2013).
[3] W. Liu, K. Yao, D. Huang, X. Lin, L. Wang and Y. Lv, Opt. Exp. **24**, 13288 (2016).
[4] W. Liang, T. Chen, L. Xinyue, L. Xudong, Y. Xiaoxia and L. Hongzhuang, J. Korean Phys. Soc. **68**, 486 (2016).
[5] J. Huang, H. Mei, K. Deng, L. Kang, W. Zhu and Z. Yao, Opt. Commun. **356**, 574 (2015).
[6] J. Cao, X. Zhao, W. Liu and H. Gu, Opt. Exp. **25**, 15299 (2017).
[7] W. Liu, W. Shi, J. Cao, Y. Lv, K. Yao, S. Wang, J. Wang and X. Chi, Optik **12**, 324 (2014).
[8] C. Liu, S. Chen, X. Li and H. Xian, Opt. Exp. **22**, 15554 (2014).
[9] A. Belmonte and B. J. Rye, Appl. Opt. **39**, 2401 (2000).
[10] V. Javier, G. Fernandez, L. Quiroga, J. Antonio and B. Tomás, Appl. Opt. **49**, 2409 (2010).
[11] L. C. Andrews, J. Mod. Opt. **39**, 1849 (1992).
[12] L. Tengtao, G. Mali, H. Lei, Q. Yuntao and X. Qiao, Appl. Opt. **51**, 7115 (2012).
[13] A. Belmonte, Opt. Exp. **16**, 6756 (2008).
[14] W. Liu, L. Wang, K. Yao, J. Cao, D. Huang and H. Gu, J. Korean Phys. Soc. **69**, 1750 (2016).
[15] H. Song, R. Fraanje, G. Schitter, H. Kroese, G. Vdovin and M. Verhaegen, Opt. Exp. **18**, 24070 (2010).
[16] C. Liu, L. Hu, Z. Cao, Q. Mu and L. Xuan. Opt. Commun. **285**, 238 (2012).
[17] Y. Qingyun, Z. Jinyu, W. Minghao and J. Jianlu, Opt. Lett. **40**, 1235 (2015).
[18] L. H. Huang and C. H. Rao, Opt. Exp. **19**, 371 (2011).
[19] Z. Li, J. Cao, X. Zhao and W. Liu, Opt. Laser Technol. **66**, 89 (2015).
[20] Z. Li, J. Cao, X. Zhao and W. Liu, Opt. Comm. **338**, 11 (2015).
[21] J. Cao, X. Zhao, Z. Li, W. Liu and Y. Song, Optik. **125**, 6142 (2014).
[22] Z. Li, J. Cao, X. Zhao and W. Liu, J. Korean Opt. Soc. **19**, 45 (2015).
[23] T. Weyrauch and A. Mikhail, Appl. Opt. **44**, 6388 (2005).
[24] W Liu, W. Shi, K. Yao, J. Cao, P. Wu and X. Chi, Opt. Laser Technol. **60**, 116 (2014).
[25] W. Liu, W. Shi, B. Wang, K. Yao, Y. Lv and J. Wang, Opt. Comm. **309**, 212 (2013).
[26] N. Roddier, Opt. Eng. **29**, 1174 (2014).